Aalto University

OPEN ACCESS

This is an electronic reprint of the original article.
This reprint may differ from the original in pagination and typographic detail.

Rodera, O.; Pärnänen, T.; Jokinen, J.; Lindgren, M.; Sarlin, E.; Kanerva, M.

Chemical ageing effects on the ply and laminate strength of a filament wound cross-ply GFRP

Published in:
Composite Structures

DOI:
10.1016/j.compstruct.2020.113508

Published: 15/03/2021

Document Version
Publisher's PDF, also known as Version of record

Published under the following license:
CC BY

Please cite the original version:
Rodera, O., Pärnänen, T., Jokinen, J., Lindgren, M., Sarlin, E., & Kanerva, M. (2021). Chemical ageing effects on the ply and laminate strength of a filament wound cross-ply GFRP. *Composite Structures*, *260*, Article 113508. https://doi.org/10.1016/j.compstruct.2020.113508

This material is protected by copyright and other intellectual property rights, and duplication or sale of all or part of any of the repository collections is not permitted, except that material may be duplicated by you for your research use or educational purposes in electronic or print form. You must obtain permission for any other use. Electronic or print copies may not be offered, whether for sale or otherwise to anyone who is not an authorised user.

Composite Structures 260 (2021) 113508

Contents lists available at ScienceDirect

Composite Structures

journal homepage: www.elsevier.com/locate/compstruct

Chemical ageing effects on the ply and laminate strength of a filament wound cross-ply GFRP

O. Rodera [a,*], T. Pärnänen [a,b], J. Jokinen [a], M. Lindgren [c], E. Sarlin [a], M. Kanerva [a]

[a] Tampere University, Faculty of Engineering and Natural Sciences, Engineering Materials Science, P.O. Box 589, 33014 Tampere, Finland
[b] Aalto University, School of Engineering, Department of Mechanical Engineering, P.O. Box 14300, FI-00076 Aalto, Finland
[c] Outotec Research Center, P.O. Box 69, 28101 Pori, Finland

ARTICLE INFO

Keywords:
ageing
finite element modelling
failure criteria
GFRP
vinyl ester

ABSTRACT

This work presents a numerical approach to multi-routines based on experiments, and, with a target to analyse strength of a cross-ply glass fibre reinforced plastics (GFRP) composite after immersion in sulphuric acid solution under pressure (5% H_2SO_4 solution, 95 °C, 15 bar). Two alternative vinyl ester resins (bisphenol A diglycidyl ether and epoxy phenol novolac) were investigated. After 0.5, 1, 1.5 and 2 years of conditioning, the specimens were mechanically tested. The multi-scale definition of the material system and its virtual conditioning were performed in a finite element (FE) model. The Hashin 3D failure criterion was implemented by coding the UMAT subroutine when using the Abaqus software. The experimental results demonstrated better performance of the bisphenol A vinyl ester resin-based GFRP when a thin barrier layer is used. The numerical results indicated that the shear strength property was the most susceptible at weak zones to present a tendency for degradation after one year of conditioning.

1. Introduction

Filament winding is a method for producing tubular, rotationally symmetric products made of composite materials. They are typically composed of glass fibre reinforced plastics (GFRP) with several applications in the chemical industry. The applications of these materials are various tubes, storage tanks and vessels that often need to seal gas or liquid inside. These operational conditions cause changes in the material's micro-structure even at low levels of deformation. Consequently, it is necessary to identify the mechanical properties (stiffness and strength) of the materials, as well as the behaviour of micro-components and the macro-structure [1,2].

In addition, the changes in the evolution of the mechanical behaviour can be degraded by the chemical environment during the operational lifetime of the material and structure. This can include the effects of moisture, temperature, pressure and chemicals that are typically referred to as ageing. The ageing due to conditioning can result in changes of the resin component (often thermoset matrix) and those occur at the covalent bonds of the molecular chains [3]. Nevertheless, an advanced resin to be used as the matrix component is vinyl ester, which possesses good corrosion resistance and mechanical properties making it suitable for many industrial applications [4–6].

Currently, the long-term mechanical performance of vinyl ester resin in fibre reinforced plastics (FRP) is being increasingly studied in numerous works. Researchers have been particularly devoted to analysing the effects of GFRP specimens subject to a sulphuric acid immersion and subsequent tensile and flexural tests. Banna and Molgaard [7] carried out a comparison between the performance of bisphenol A epoxy vinyl ester and polyester (pure) resins. The results demonstrated superior capabilities for bisphenol A epoxy vinyl ester resin in terms of bending and tensile tests, and a lower penetration of the acid medium into the micro-structure. Kootsookos and Burchill [8] studied the corrosion resistance of a certain vinyl ester resin by means of an analysis of variances. They concluded that fibre volume fraction affected ageing, which stabilised after six months of conditioning. Similarly to the acid-sulphuric immersion, Cabral-Fonseca et al. [9] applied different water immersion conditions and, interestingly, found that flexural properties were more affected by conditioning than tensile and shear (interlaminar) properties.

Most of the research works involve loading conditions in tension or bending leading to specific types of failure. Specifically, under tensile tests in the longitudinal direction, the cross-ply laminate fails due to transversal damage and then longitudinal damage [10]. This can be also altered by the ageing effects and, thus, the material modelling is

* Corresponding author.
E-mail address: oscar.roderagarcia@tuni.fi (O. Rodera).

https://doi.org/10.1016/j.compstruct.2020.113508
Received 14 February 2020; Revised 6 December 2020; Accepted 16 December 2020
Available online 25 December 2020
0263-8223/© 2020 The Authors. Published by Elsevier Ltd.
This is an open access article under the CC BY license (http://creativecommons.org/licenses/by/4.0/).

required to accurately predict and analyse the degradation mechanisms. This can be done by taking into account the design factors (e.g. reinforcement type), defects in micro-structure (such as voids), boundary conditions and failure modes.

To predict ageing, advances have been made in the modelling of composite plies. Barbero and Damiani [11] predicted the tensile strength of GFRP by a model based on curve-fitted data collected from the literature. Krishnan and Oskay [12] proposed a multi-scale damage model to capture the compression-after-impact response of GFRP first immersed in seawater. Naya et al. [13,14] obtained significant results by using computational micromechanics that were implemented in a finite element (FE) modelling. The deformation and fracture mechanisms were simulated in a ply of carbon FRP and under different environmental conditions. The results were compared to the implementations of the Puck [15] and LaRC04 [16] failure criteria. Their damage evolution models were applied up to ultimate failure and good correlation was obtained, especially, with the LaRC04 criterion in terms of the compression strength. Typically, the onset of mechanical failure is the limiting factor applied to design procedures. In consequence, major work was carried out to evaluate the performance of failure criteria through the World Wide Failure Exercise (WWFE) [17]. This baseline work focused on elucidating the three-dimensional (3D) stress state and the failure of laminates during the second exercise (WWFE-II) [18].

This paper presents an experimental and numerical analysis of a filament-wound GFRP composite. The target is to evaluate experimental results for the material modelling subject to tensile loading case and understand the major tendency of degradation of the strength properties for the condition affected by ageing. The material was aged in a sulphuric acid environment (5% H_2SO_4 solution, 95°C, 15 bar) for a maximum of two years. A detailed experimental test programme was carried out including uni-axial and flexural tests. A micromechanical homogenisation method and FE modelling were employed to simulate the mechanical response of GFRP specimens. The strength analysis was implemented by means of the Hashin 3D failure criterion [19–21] as damage activation functions through the UMAT subroutine (Abaqus/Standard).

2. Material and methods

2.1. Laminate preparation and manufacturing defects

This present work investigated two vinyl ester resins: Derakane 455–400 (bisphenol A diglycidyl ether (DGEBA) based resin, supplied by Ashland) and Atlac E-Nova FW 1045 (epoxy phenol novolac (EPN) based resin, supplied by DSM). Atlac E-Nova FW 1045 resin (named resin-A) has generally good thermal and chemical resistance. Derakane 455–400 resin (resin-D) shows high flexibility and slightly reduced chemical and heat resistance. The GFRP with resin-D has presented a typical mass increase in sulphuric acid solution immersion for one year, while the GFRP with resin-A presented rather low mass increase [22].

Fig. 1 shows the manufacturing procedures and material processing of the GFRP specimens in this study. The dimensions of the filament-wound tubes are presented in Fig. 1, as well as the laminate lay-ups of the structural layer. In addition, the tubes were manufactured with barrier layers (outer parts), which carried out the protective function against chemical attack from the medium inside. Therefore, both types of layers constituted the section of the specimens.

The tubes were manufactured with three different configurations depending on the sequence and thickness of the barrier layers. According to these characteristics, the tubes were categorised by Sections 1–3 (see Fig. 2). The barrier layers were made with nine layers of chopped strand mat (M723A, 300 g/m^2, Owens Corning) forming a thickness of 6 mm. The inner surfaces of the specimens were covered with a layer of ECR-glass surface mat (M524-ECR30S, 30 g/m^2, Owens Corning).

The structural layer was manufactured by using the winding technique and a lay-up of $[90_2/0/(90/0)_{14}/90_2/0/90_2]$ equal for all the tube configurations. The 0° plies were based on 20 layers of winding roving (U480 R25HX14, 480 g/m^2, 3B-fibreglass) and the 90° plies on 16 layers of axial roving (UD256 R12-256-T, 256 g/m^2, Ahlstrom). The UD256 reinforcement was wound on a mandrel in the perpendicular direction with respect to the longitudinal axis of the tube (90°). The whole tube length was covered by a circumferential winding (see Fig. 1).

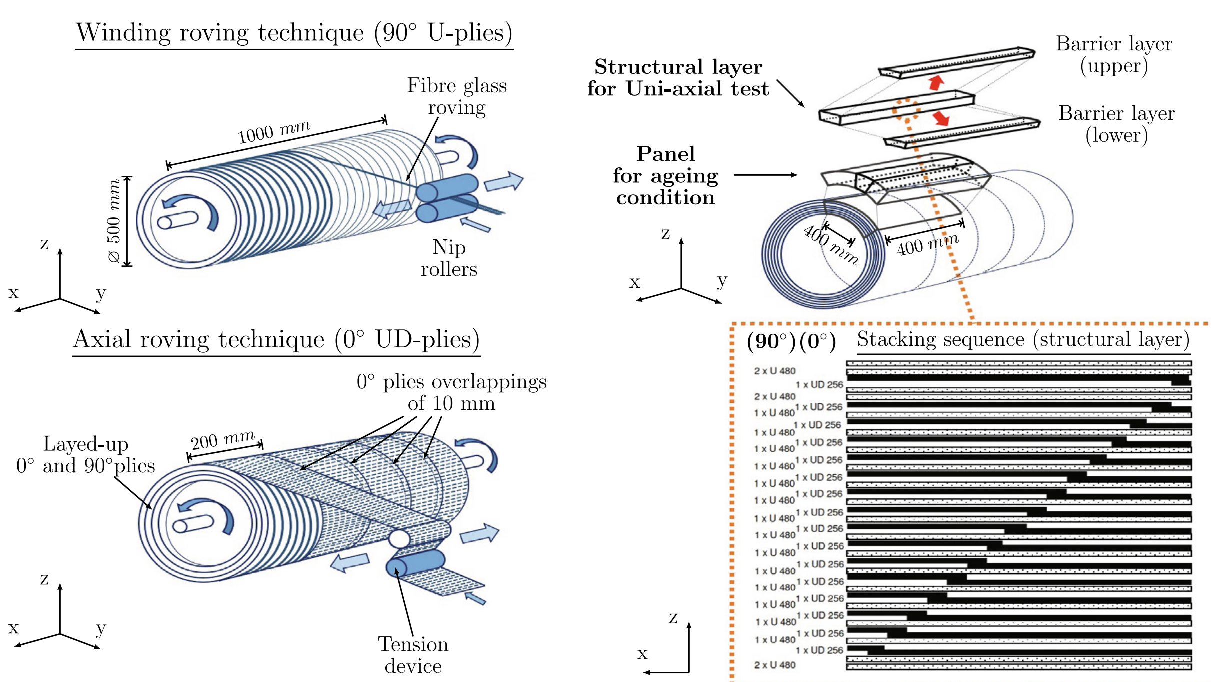

Fig. 1. Manufacturing procedures and lay-up for the specimens in this study (longitudinal direction is defined as the 0° direction).

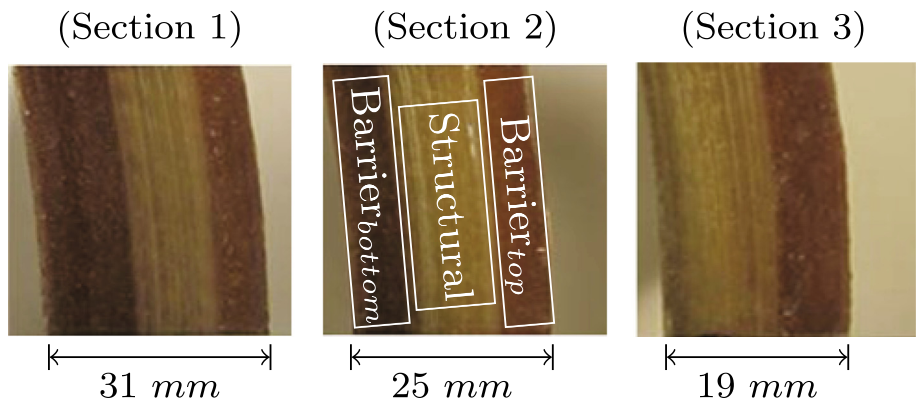

Fig. 2. Cross-sections of the GFRP-A and GFRP-D panels, categorised by means of the thickness and sequence of barrier layers as Sections 1–3.

The U480 reinforcement was formed by unidirectional tapes (UT) of 200 mm width, orientating its fibres in the longitudinal direction (0° angle). The UTs were positioned in such a way that the ends nominally overlapped 10 mm in each rotation. This overlapping repeated itself every 190 mm, generating a patterned defect in the lay-up through the thickness (see Fig. 1). The properties of the glass fibres for both kinds of ply are shown in Table 1.

2.2. Experimental specimens

2.2.1. Chemical conditioning

Once the tubes were manufactured, GFRP-A and GFRP-D panels (with the corresponding sections) were cut out in a size of 400×400 mm^2 and sealed with resin at the edges. Subsequently, the panels were conditioned by immersion procedure at a temperature of 95 °C and a pressure of 15 bar (see Fig. 3). The sulphuric acid–water bath was based on 5% H_2SO_4 solution. For avoiding harsh corrosion in the metallic parts of the system, 0.5 g/l of $Fe_2(SO_4)_3$ was added to act as an inhibitor. Series of GFRP panels were removed from the reactor after 0.5, 1, 1.5 and 2 years of conditioning and, subsequently, the mass was measured ($\pm 1\ g$). Different reactors were used according to the resin used and no specimens already conditioned were submerged back.

Additionally, the same process of conditioning was carried out with pure resin specimens (Resin-A and Resin-D) but limiting their ageing up to one year. The results for the first measurements are reported in earlier works [22,2].

2.2.2. Resin testing

The pure resin specimens (Resin-A and Resin-D) were subject to a three-point bending test according to ISO 178:2010 [24]. The specimens had a nominal thickness of 6 mm and planar dimensions of 15mm×80mm. They were tested with an universal testing machine (Electropuls E 3000, Instron) with a 3 kN load cell and computerised control (WaveMatrix, Instron). The displacement rate was 2 mm/min. The testing was carried out for six non-aged specimens and six

Table 1
The properties of micro-components of the material as provided by the manufacturers [22,23].

Resin	Density (kg/m^3)	Ultimate strain* (%)	Tensile modulus (GPa)	Poisson's ratio (–)	Tensile strength (MPa)
Resin-A	1145	5–6	3.3	0.3	85
Resin-D	1040	4	3.5	0.32	88
Fibre**	Density (kg/m^3)	Areal weight (g/m^2)	Tensile modulus (GPa)	Poisson's ratio (–)	Tensile strength (MPa)
Glass (U480)	2620	480	79	0.2	2750
Glass (UD256)	2540	256	72.4	0.2	2450

* Elongation at yield.
** Ultimate strain of 2.6% [25].

Fig. 3. I) Section matter of the tube; II) panel for conditioning (one quarter of smaller tube section); III) reactors of the conditioning; IV) aged specimens after conditioning (structural + barrier layers), V) specimens for mechanical tests (structural layer).

specimens with a condition after one year-immersion. The average flexural modulus, proof stress at 0.05% plastic strain and ultimate strength were determined; details of the test procedures and analysis methods are given in a previous work [2].

Similarly, a procedure of prior ageing and following mechanical experiments was carried out on pure glass fibres. However, measured data could not be obtained after an ageing condition of more than two weeks. The 5% H_2SO_4 solution resulted in a harsh environment for the fibres [25].

2.2.3. Tensile testing

The GFRP panels were cut in narrow pieces without the barrier layers after the ageing (see Fig. 3-V). They were categorised as GFRP-D and GFRP-A and per section (Sections 1–3). The specimens were subjected to uni-axial tensile testing in the longitudinal direction at a room temperature in accordance with ISO 527-4 [26]. End tabs were not used. The tests were performed using a servo–hydraulic tester (Dartec 100 kN) with a displacement rate of 2 mm/min. The elongation was measured using an extensometer (50 mm gauge length, MTS). For the specimens with resin-A, five tests were made for each of the three sections of the barrier layers in each of the five immersion times of conditioning (virgin + four aged cases). The same procedure was carried out for the specimens with resin-D by performing a total of 150 tests. The dimensions of the specimens were 25 mm in width and 250 mm in length, with a nominal thickness of 14 mm (Fig. 1). The behaviour of the tensile specimens was determined by means of the ultimate strength, Young's modulus and proof stress based on a proportionally limit of 0.05% (see Fig. 4).

2.3. Numerical analysis with multi-routines

A numerical framework of multi-routines, calibrated with the experiments, was set to study the ageing effects on the ply properties (strengths) of the laminate. The configuration of two multi-routines was designed to model the heterogeneous material and analyse variations in the response, under the tensile loading, due to the chemical conditioning. The numerical approach was characterised by the sensitivity and flow of material data to predict the virgin and conditioned behaviours of the specimens. The GFRP-D Section 1 was selected for the analysis as a consequence of its response to the chemical attack (see Section 3). The analysis is limited to the virgin and the 1-year conditioned specimens.

The first numerical multi-routine (on the left, Fig. 5) defined the material with multi-scale basis at the linear-elastic domain. The connection between micro-constituents and ply properties was made by the homogenisation approach of the Halpin-Tsai method [27]. Through its rule of mixture, the elastic constants of the ply were averaged by taking the volume ratio of the composition (volume fraction of fibres, V_f) and the mechanical properties at the micro-scale (see Table A.8 in the Appendix). Consequently, the homogenised properties were plugged into a FE solver, which performed the computing of the real specimen. This linking process made the ply properties dependent on the micro-constituents and the FE model. The prediction of their (aged or not) response required two fitting procedures, referred to as 'composition' and 'stiffness' loops. These loops involved iterative operations of comparison between the numerical and experimental results.

The second multi-routine (right side, Fig. 5) focused on the survey of the strength properties in the FE model under the ageing condition of one year. The simulation of the conditioning was carried out by a sampling function of the virgin properties at the ply level. This step generated sequences of (conditioned) data that were processed through an inputting procedure giving rise to a 'strength' loop. This was based on iterative entries of the strength properties into the FE model in order to analyse their effect on the failure values.

The numerical analysis of ageing effects through the approach of the multi-routines involved the following crucial presumptions: I) The effects of ageing are assumed not to alter the linear-elastic behaviour at the load level of the simulations, though this might not fully hold true in reality. II) The laminate structure is solid and intact and the 3D failure criterion can be used to determinate the 'non-critical' stress-strength relation for each failure mode in the filament-wound plies. III) The ageing condition does not affect the nominal fibre volume fraction (e.g. through removal of material) used in the Halpin-Tsai equations.

2.3.1. Material definition loop and laminate modelling

The first multi-routine generated the composition and stiffness loops for the non-aged and 1-year ageing cases, respectively. The

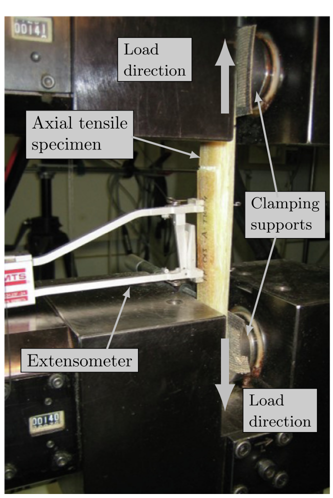

(a)

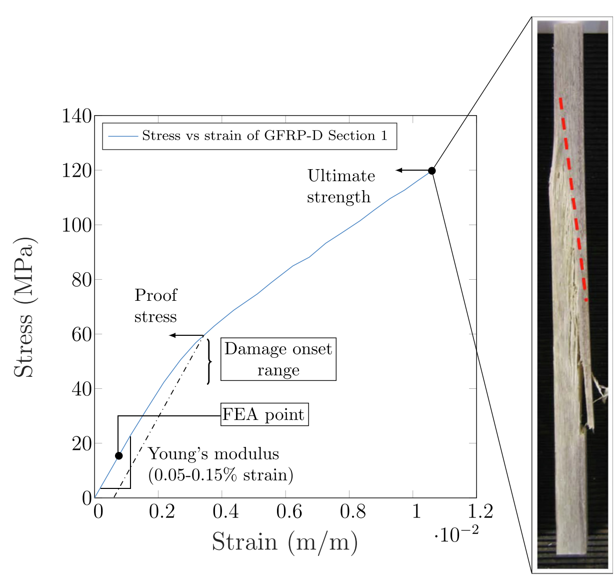

(b)

Fig. 4. The system of the uni-axial tensile test and description of the behaviour: (a) Set-up, and, (b) stress-strain curve and the definitions used in the study. The detail view shows the pattern of defects (diagonal red dotted line) on the tested specimen at the ultimate failure point.

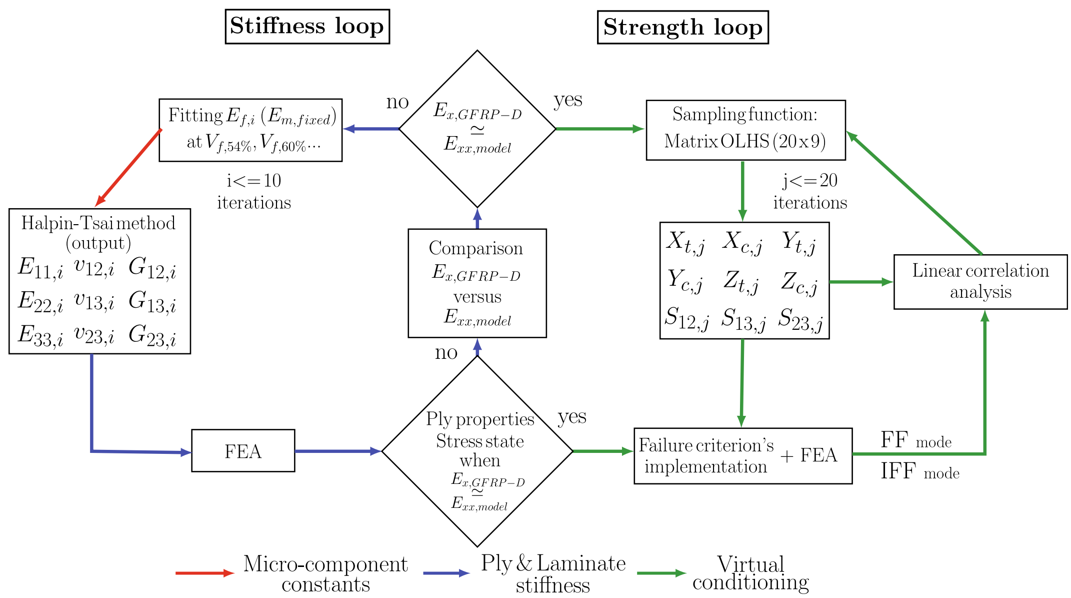

Fig. 5. Numerical multi-routines for the (virtual) conditioning of the stiffness and strength properties, including the modelling of material at micro and meso scales.

fitting variable for each process was the longitudinal Young's modulus (E_x) obtained from the tensile (virtual) test.

For the non-aged case, the composition loop focused firstly on calibrating the fibre volume fraction (V_f). Initially, the first V_f value was determined by the experimental data and the following formula:

$$V_{f,GFRP-D} = \frac{\omega_{f,GFRP-D} \cdot \rho_{GFRP-D}}{\rho_f} \tag{1}$$

where the fibre mass fraction ($\omega_{f,GFRP-D}$) can be found in a previous research [22] and the densities ($\rho_{f,GFRP-D}$) in Table 1. The densities of the two different fibres were presumed to be equal $\rho_f = 2.58$ g/m^2, giving a value of $V_{f,GFRP-D} = 53\%$. The first set of properties at the ply level were created by inputting the calculated $V_{f,GFRP-D}$ value and the virgin constants of the micro-constituents (Table 1) into the Halpin-Tsai equations (see Table A.8 of Appendix). This method involved the 'reinforcement' parameters that require a specific adjustment. These factors can indicate the degree of matrix reinforcement by the fibres, and allow to consider issues (e.g. matrix defects, fibre distribution, inter-phases) in the realistic (homogenised) micro-structure.

For the initial non-aged case, the micro-constituents' constants were fixed to their original values. Table 2 shows the first set of the nine elastic constants of the ply for GFRP-D Section 1 ($V_f = 53\%$). Subsequent iterations in the composition loop were based on the adjustment of V_f in the Halpin-Tsai equations.

Once the definition at the ply level was done, the ply properties were input into the FE software (Abaqus/Standard), which simulates the tensile test in the routine. The geometry of the model specimen was based on the measurements of the real specimen: 25 mm wide, 250 mm long, and 14 mm thick (nominally) ($t_{nominal}$). The thickness of each ply in the lay-up was calculated by means of the following formulas:

Table 2
The nine non-aged elastic constants (3D) of GFRP-D Section 1 ply determined by using the stiffness loop (Fig. 5) with $V_f = 53\%$.

E_1 (GPa)	$E_2 = E_3$ (GPa)	$\nu_{12} = \nu_{13}$ (–)	ν_{23} (–)	$G_{12} = G_{13}$ (GPa)	G_{23} (GPa)
43.52	7.09	0.25	0.37	2.69	2.58

$$t_{0^0-ply} = \frac{w_{UD256} \cdot t_{nominal}}{w_{total}} \tag{2}$$

$$t_{90^0-ply} = \frac{w_{U480} \cdot t_{nominal}}{w_{total}} \tag{3}$$

where finally $t_{0^0 ply} = 0.262$ mm and $t_{90^0 ply} = 0.491$ mm; w_{total} was defined as ($16 \cdot w_{UD256} + 20 \cdot w_{U480}$). The subtotal areal weight for the UD256 and U480 plies can be found in Table 1.

The boundary conditions for the FE model were based on a mechanism that clamped the right end of the model and applied a displacement at the left one (see Fig. 6). The FE model was subjected to a displacement of $u_x = 0.1e\text{-}03$ m ($\varepsilon_{11} = 0.67e\text{-}03$ m/m) to keep the specimen behaviour at the linear-elastic domain. The output data was collected from the FE model in a similar way to the real experiment (points of extensometer arms). The mesh was discretised by a total number of 916,160 elements of type C3D8, eight-nodes linear brick, fully integrated. The default hourglass control method was chosen to reduce zero-energy modes, since it provided a good coarse mesh accuracy under the applied loading condition. The mesh was based on one element per 0° ply and two elements per 90° ply. This element mesh provided results for predicting stress values in regions near to free-edges and 'weak zones' (see Fig. 6).

The weak zones in the FE model represent the manufacturing defects that are repeated through the lay-up in each 0° ply. As shown in Fig. 1, these defects were provoked by the overlapping between 0° plies along the 1000 mm of GFRP tube length. Fig. 7 (left-side) shows this overlap effect between 0° plies (as expected). In addition, the defects of resin gaps were also detected as a portion of the 0° plies along the longitudinal direction and at locations where overlaps should have taken place (right side, Fig. 7). This might be due to the incorrect position of the overlapped UTs. These defects influenced the meso-structure leading to higher deformations as the loading was applied. In consequence, they were considered to behave as the critical points of the micro-structure.

In order to establish the basis for the modelling of the weak zones, an analysis of the micro-structure was done through the micro-graphs, as illustrated in Fig. 7. The length observed for the case of the overlap was of 10 mm, and similar dimensions for the gap defects.

The micro-graph of the overlap defect (left-side, Fig. 7) shows mainly the presence of stitches of the UD256 ply, a high void content

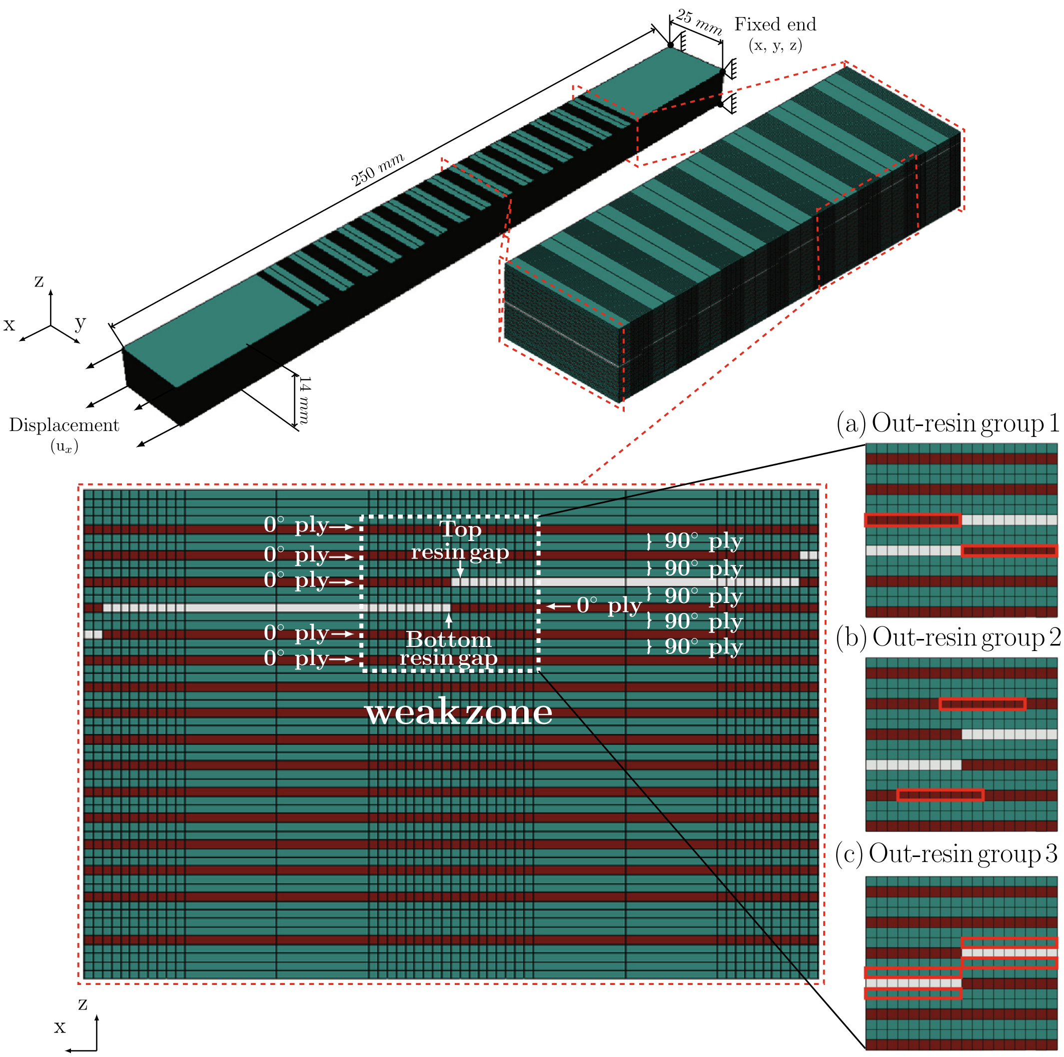

Fig. 6. The modelling of the tensile specimen with resin gaps in the lay-up. The set of elements for failure analysis are in sub-picture (a) out-resin group 1, (b) out-resin group 2 and (c) out-resin group 3.

and resin-rich zones around the overlapping line. According to the micro-graph of the gap defect (right-side, Fig. 7), full zones of resin can clearly be observed. The resin-rich zones at the inter-laminar face can not be disregarded, since their presence might affect the longitudinal load-bearing capacity. These zones could also result in higher strains perpendicularly to the loading condition in 0° plies but, also, in shear direction for the 90° plies.

As a consequence, the weak zones were modelled as resin gaps by considering them as primary defects in the design of the meso-model (see Fig. 6). Whereas the void content was considered in the definition of the ply properties through the ξ factor and adjusted fibre volume fraction in the Halpin-Tsai equations. The resin-rich zones and voids required that the values of the matrix-dominated moduli i.e. transverse and shear module were indirectly estimated in the semi-empirical method. It has been reported that the effects of the voids lead to significant degradation of the stiffness properties with respect to virgin conditions [28,29]. The mesh in the weak zones was refined through the thickness direction in order to obtain accurate results.

Finally, the virtual conditioning of one year over the material was similarly simulated by using the stiffness loop. This consisted of an iterative process where the routines focused on varying only the Young's modulus of the fibre constituent (see Fig. 5). The aged elastic constants could be collected from the experiment and calibrated in the loop. The adjustment in the calibration kept the material composition and geometrical characteristics unchanged as defined previously for the FE model in the non-aged case. The voids were also assumed to affect similarly to the transverse and shear constants under the exposure of the conditioning, as has been observed to be the case in composites in the current literature [30].

2.3.2. Conditioning of strength properties and failure criterion

The second multi-routine carried out the virtual conditioning of 1-year by means of the strength loop. This iterative process worked only on the properties at the ply level, with a subsequent plugging into the FE model. This procedure required the properties and characteristics of the model that were defined in the first multi-routine for the non-aged condition and the one-year ageing condition.

The nine strength properties that were collected from the ESAComp software's library [23], were the reference values of our sensitivity analysis. The reference represents the original, standard level of strength. The effects of the resin gaps and voids were not separately analysed. Research works have demonstrated that the void content produce similar mechanisms of degradation than ageing, especially on the matrix-dominated properties [28,31]. The reference values of the strengths can be found in Table 3.

Subsequently, the (original) properties were processed by using the Optimal Latin Hypercube Sampling (OLHS) [32]. This method generated a set of optimal values for each strength variable within a

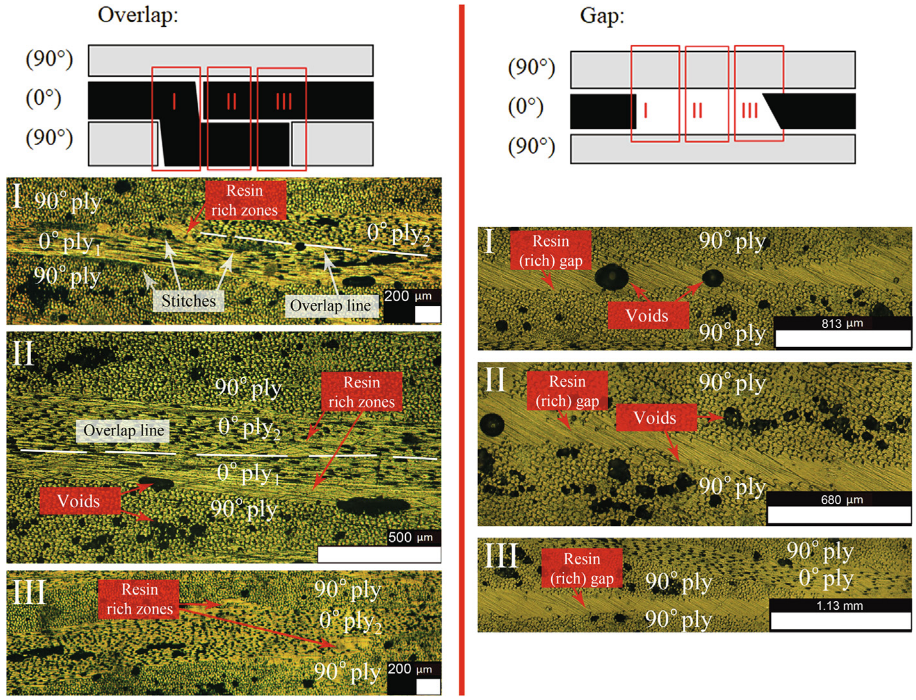

Fig. 7. Micro-graphs about defects of the overlap and gap between two adjacent 90° plies at the beginning (I), the midway (II) and the end (III) of their arrangement.

Table 3
The non-aged ply strength for the GFRP-D Section 1 from ESAComp library [23].

X_t (MPa)	X_c (MPa)	$Y_t = Z_t$ (MPa)	$Y_c = Z_c$ (MPa)	$S_{12} = S_{13}$ (MPa)	S_{23} (MPa)
1100	675	35	120	80	46.15

pre-set range simulating its (virtual) conditioning. The bounds of the sample were fixed to a ±26% deviation with respect to the original values by considering the maximum degradation of the XX_t for the GFRP-D Section 1 (blue-striped bar, Table 9). Furthermore, the range of values was divided in 20-161 equal intervals. This processing of data generated a matrix of nine columns (properties) by an example list of 20 (conditioned) values (see Table A.10 in Appendix for exact values). Consequently, 20-161 iterations were involved in the strength loops, associating one simulation of the tensile problem per each row of the extracted properties. The virtual conditioning generates a series of data to observe their effects on the failure values of the model.

The Hashin 3D failure criterion [20] was selected to determine such points of the behaviour curve at which the critical zones of the FE model (weak zones) are still able to sustain loading. The implementation of the criterion into the FE model was carried out by using the Abaqus user subroutine UMAT [33]. The user-defined material and failure modes were run for each 90° and 0° ply. However, the criterion implementation was not applied into the resin gaps due to the findings of the WWFE-II. The involved failure theories in this referencing exercise obtained no accurate and equal results in the test case for a polymer material of homogeneous section [18].

Hashin's theory represents a limit criterion (comparison between stresses and corresponding strengths properties) and an interactive criterion (it is expressed by a polynomial form involving all stress components). Furthermore, it describes the fibre failure (FF) mode and matrix/inter-fibre failure (IFF) mode separately. The FF mode equations are functions of the strength parameters and the stress tensor components of each ply in the local coordinate system (LCS), σ_{11}, σ_{12}, σ_{13}; and the IFF mode equations depend on the strength parameters and the stress tensor components of the LCS, σ_{22}, σ_{33}, σ_{12}, σ_{13}, σ_{23} (see Table A.9 of Appendix). Although Hashin's criterion does not predict the compressive modes for the matrix failure well (due to non-consideration of the shear strength), it was considered suitable for the current tensile test case [21,34,15].

The outputs of the failure criterion were analysed in three sets of elements of the weak zones targeted to obtain the most critical values. The selection of the elements for output was based on the obtained values from the stress field. Depending on the failure modes (FF and IFF), these groups of elements involved particular values according to their location in the plies. They were named as out-resin group 1, out-resin group 2 and out-resin group 3 (see Fig. 6). Finally, for each of the element sets, a process of data collection was carried out to analyse their linear correlation with respect to the generated properties in the OLHS. For that, the failure values were defined as the linear correlation factors (LCF) for the failure criterion's value (range 0...1).

3. Results and discussion

3.1. Resin ageing

The three-point bending tests showed that resin-A reached higher level of ultimate stress but experienced a slight reduction of stiffness after the 1-year conditioning whereas for resin-D both ductility and strength were increased (Table 4).

The effects of the ageing were more pronounced for resin-D than resin-A. The explanation for these results might stem from post-curing caused by the elevated temperature during conditioning.

3.2. Tensile test results

The results are summarised in stress–strain curves (Fig. 8) and in degradation ratios where the three mechanical properties are normalised with respect to the non-aged ones (Fig. 9). All the specimens

Table 4
Experimental results i.e. mechanical properties of resin-A and resin-D-based pure specimens (non-aged and 1-year aged cases) by three-point bending test.

Mechanical properties	Non-aged case		1-year ageing condition		Incremental effects	
	Resin-A	Resin-D	Resin-A	Resin-D	Resin-A	Resin-D
Young's modulus (GPa)	3.2 ± 0.1	3.5 ± 0.1	2.8 ± 0.2	2.9 ± 0.1	(–) 15%	(–) 18%
Proof stress (offset 0.05%) (MPa)	80*	n/a* * *	51**	68 ± 17	(–) 36%	n/a* * *
Ultimate strength (MPa)	66 ± 8	72 ± 3	71 ± 10	96 ± 20	(+) 8%	(+) 33%

* One specimen ** Two specimens * * * No plastic strain for offset.

showed essentially brittle behaviour until the ultimate load was reached.

The GFRP-A and GFRP-D series presented a gradual decrease in ultimate strengths over the two years of conditioning. The strength values of GFRP-D decreased less than those of GFRP-A.

Regardless of the type of resin, the specimens with the thinnest barrier layer (Section 3) presented generally lower values for the ultimate strength than the thicker sections (Sections 1 and 2). However, the GFRP-A Section 1 (having originally the thickest barrier layers) led to higher degradation than any section of the GFRP-D specimens up to the 1-year conditioning. This demonstrated the better resistance of the GFRP-D specimens to the chemical conditioning than the GFRP-A specimens.

The proof stress values were in the range of 40 MPa to 65 MPa. At the beginning of the conditioning, the highest differences of degradation between GFRP-A and GFRP-D were in the range of 17 to 22%. However, this difference diminished after one year, to a range between 6 and 10%. For the Young's modulus, the maximum degradation was found in the Section 3 of GFRP-D, which showed a 25% decrease after 1.5 years of conditioning. In summary, most of the stiffness loss occurred up to a one-year ageing condition through the test series.

The conditioning in the sulphuric acid–water solution could have led to the physical ageing [1]. In addition to the chemical effects, the presence of small molecules leads to swelling that might change the micro-structure. Therefore, the mass increase was measured to study the effect per section, as shown in Fig. 10. The panels had initial level of mass range of 4959–8193 g. The GFRP-D middle sections (Section 2) gained approximately twice as much mass as the thickest sections of the GFRP-A per measurement point. All the curves had an increasing trend towards the end of the conditioning. Therefore, specimens did not reach the saturation point after two years.

3.3. Simulated tensile test results

The results of the fitting procedure for the composition (non-aged case) and stiffness (1-year ageing case) loops are shown in Fig. 11. The stress strain curves show the prediction of the FE simulation with respect to the experimental results.

For the non-aged condition, the composition loop involved adjusting the V_f of ply in three steps (40%, 53% and 60%). Fig. 11 a shows the three geometrical configurations for the modelling of resin gaps (weak zones). The loop did not involve alteration of the micro-component constants in their virgin status but only V_f in the Halpin-Tsai equations (ply level). Furthermore, this method required the fitting of its parameters (ξ_s and ξ_t) in the predictions of the transverse and shear elastic constants. Usual values for these parameters are ξ_s

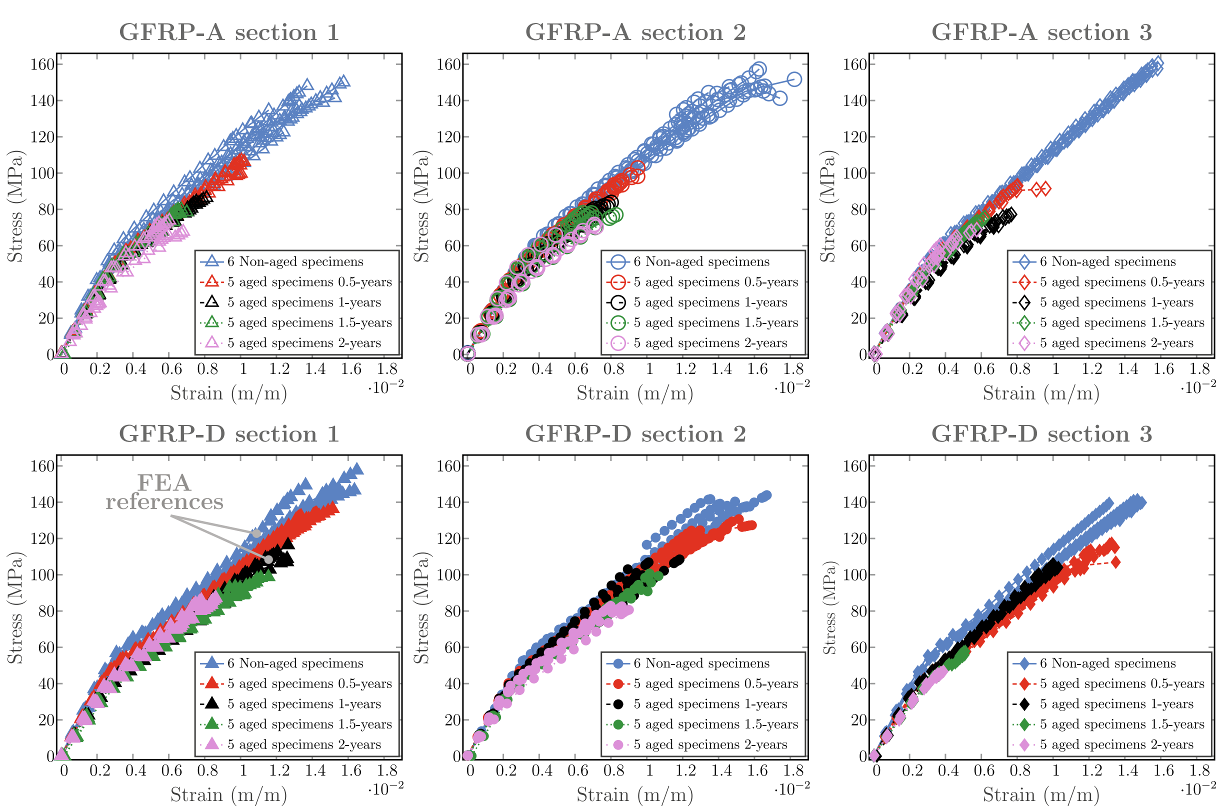

Fig. 8. Experimental stress–strain curves of the GFRP-D and GFRP-A specimens with the Sections 1–3 under the tensile testing.

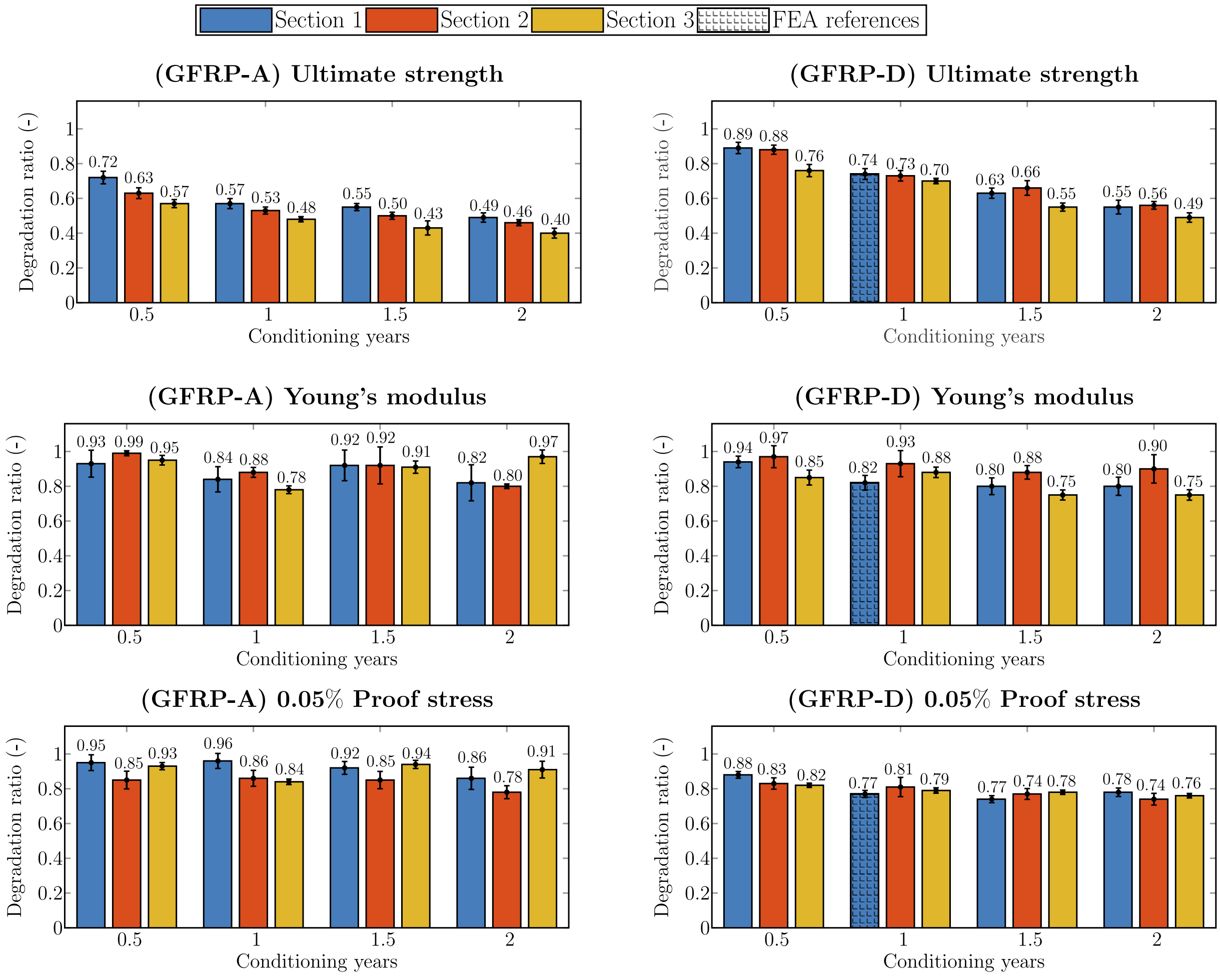

Fig. 9. Degradation ratios of the mechanical properties of different specimen series. The left column represents GFRP-A sections and the right side GFRP-D sections.

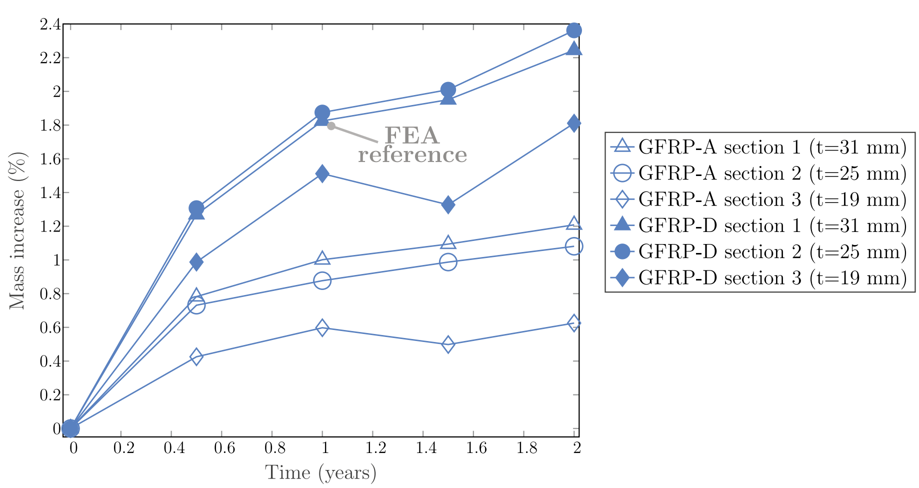

Fig. 10. The mass increases observed over the ageing in the GFRP-A/D panels.

= 2 and ξ_t = 1, which have been demonstrated to achieve accurate predictions under normal conditions without defects in the microstructure [35]. For the current case, the value of $\xi_{t,s}$ = 0 resulted in the lower bound values (43% lower for E_2 = E_3 and 30% lower for G_{12} = G_{13}) to account for void defects and resin rich zones outside resin gaps.

As shown in Fig. 11 and Table 5, the fitting procedure of the longitudinal Young's modulus was reached with the value of V_f = 60%. The initial design for the resin gap (upper configuration) resulted in being the most proper under the structural characteristics. Consequently, the updated nine elastic constants of the ply were obtained for the non-aged case, as given in Table 6. It should be noted that the adjustment

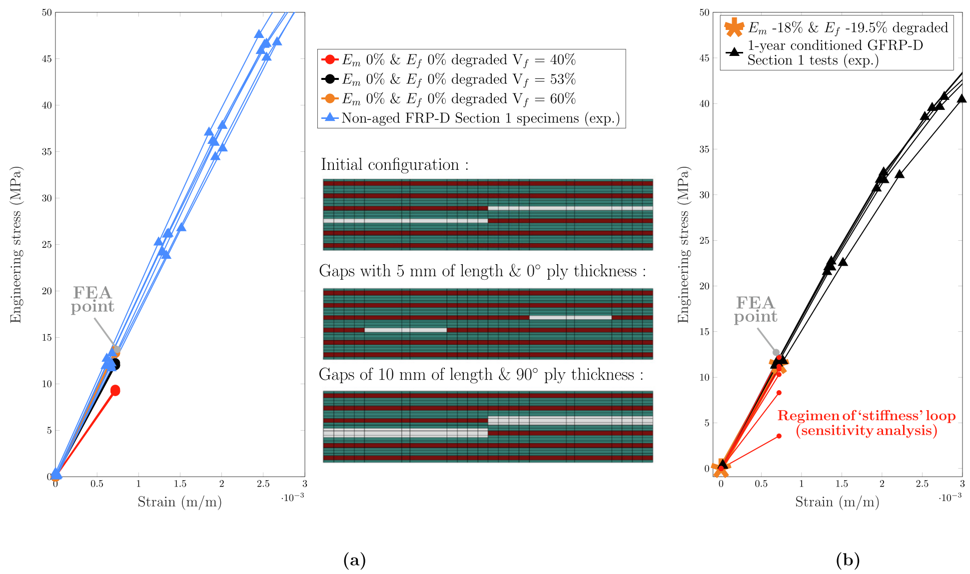

Fig. 11. The fitting of the numerical curves (longitudinal stiffness) of the GFRP-D Section 1 specimen to the experimental ones: (a) Non-aged condition, and, (b) 1-year ageing condition.

Table 5
Experimental (average ± standard deviation) results of the tensile testing; and the stiffness of the simulated model at the linear-elastic regimen (for non-aged condition).

Specimen	Young's modulus (GPa)	0.05% proof stress (m/m)	Ultimate strength (MPa)
GFRP-A Section 1	19.1 ± 1.6	59.9 ± 2.2	143.1 ± 4.9
GFRP-A Section 2	17.4 ± 0.1	63.5 ± 3.0	154.1 ± 4.9
GFRP-A Section 3	18.0 ± 0.4	60.0 ± 0.9	157.4 ± 2.7
GFRP-D Section 1	19.2 ± 0.7	60.4 ± 0.9	149.1 ± 4.3
GFRP-D Section 2	17.6 ± 0.7	59.8 ± 2.2	142.5 ± 2.7
GFRP-D Section 3	18.9 ± 0.6	60.0 ± 0.5	147.2 ± 1.8
GFRP-D Section 1 FE model	18.51	n/a	n/a

of V_f here involves effects of voids that are implicitly included in the experimental test data. Therefore, the adjusted V_f and V_m are effective values for modelling.

Fig. 11 a and b also show the points of the test simulation for the tensile test and at which the failure analysis was carried out.

The target (input) load for the non-aged case, $\sigma_x = 14.06$ MPa and $\varepsilon_x = 0.67\text{e-}03$ m/m, and for the one-year ageing condition, $\sigma_x = 12.25$ MPa and $\varepsilon_x = 0.72\text{e-}03$ m/m.

Fig. 12 introduces the six components of the stress tensor in the modelling of the weak zone that were obtained by inputting the (non-aged) ply properties (Table 6).

The stress results show that the presence of the resin gaps locally produces high deformations in the 0° and 90° plies and their surrounding. It should also be pointed out that the shear component σ_{12} peaks at the edge of the specimen due to the free-edge effects [36].

The stress results will be discussed in detail to analyse their influence on the failure study for the non-aged condition in Section 3.4.

Table 6
The nine (non-aged) elastic constants of a ply in the GFRP-D Section 1 (with V_f = 60%).

E_1 (GPa)	$E_2 = E_3$ (GPa)	$\nu_{12} = \nu_{13}$ (–)	ν_{23} (–)	$G_{12} = G_{13}$ (GPa)	G_{23} (GPa)
48.80	8.20	0.25	0.38	3.12	2.98

The fitting of the longitudinal Young's modulus for the 1-year virtual conditioning is shown on the right in Fig. 11. This process, similarly to the non-aged one, calculated the nine elastic constants of a ply but by using the stiffness loop (values in Table 7). The adjusting of the fibre's Young's modulus in this loop finally resulted in a degraded value (due to ageing) of 19.5% with respect to its virgin value. The Young's modulus of the resin was directly fixed by taking the experimental value from Section 3.1 (i.e. 18% degraded value).

3.4. Sensitivity of the determined failure to parametric strength variation

Before the virtual conditioning, it was necessary to analyse the stresses and the values of the failure modes at the non-aged condition of the FE model. For that, Fig. 13 shows the meso-model of a baseline weak zone, composed by the cross-plies (0°/90°/0°), with the corresponding failure modes. The implementation of the criterion involved, besides the defined stiffness properties, the non-aged stress field (Fig. 12) and the inputting of the virgin strength properties (Case 0 in Table A.10). By following the division of the Hashin criterion into the two modes, the failure ratios by longitudinal deformations were analysed for the FF mode in the 0° plies and for the IFF mode in the 90° plies. Similarly, the failure ratios by transverse deformations were analysed for the FF mode in the 90° plies and for the IFF mode in the 0° plies.

Regarding the longitudinal deformations, the representative element of the 0° plies presented the highest values of stress for the σ_{11} component. In the 90° plies, the maximum (absolute) stress values were achieved by the σ_{22} component at the second element(s) with respect to the datum plane (in red colour). In the same plies, relevant values (i.e., maximum local stresses) were achieved by the σ_{23} component (blue colour) at the first element(s) that resulted in a diagonal deformation. It should be noted that the high σ_{23} values were due to the influence of the resin gaps. According to the results, the IFF mode in the 90° plies reached the highest failure values of the weak zone's modelling. This took place in the first two elements (to the left and right with respect to the datum plane) that were under and on top of the resin gaps. Therefore, the results demonstrated that this type of stress-deformation mechanism happens mainly due to the stress components σ_{22} and σ_{23}. This might typically constitute the interlaminar failure that occurs at higher levels under transverse tensile stress in the 90° plies of a cross-ply (at the failure plane parallel to fibres) [37].

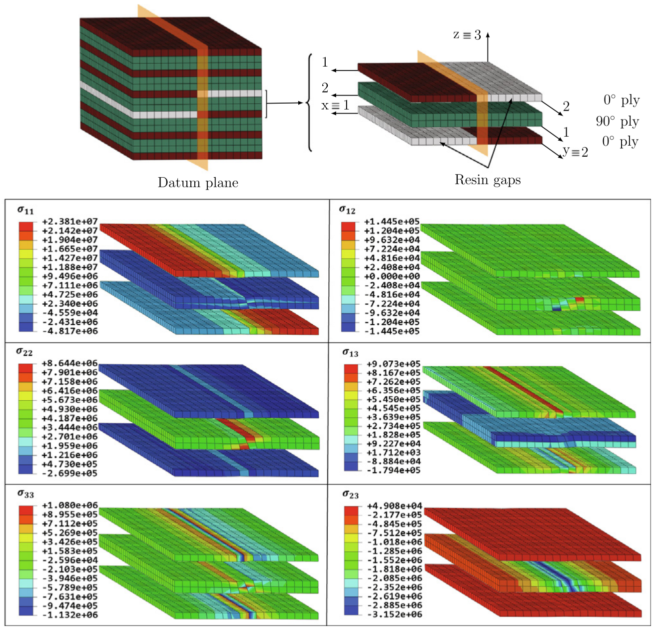

Fig. 12. Results of the stress tensor components at the weak zone for the non-aged condition at overall load condition of $\varepsilon_{11} = 0.67e\text{-}03\ m/m$ in LCS (units in Pa).

Table 7
The nine elastic constants of the GFRP-D Section 1 at the 1-year ageing condition ($V_f = 60\%$).

E_1 (GPa)	$E_2 = E_3$ (GPa)	$\nu_{12} = \nu_{13}$ (–)	ν_{23} (–)	$G_{12} = G_{13}$ (GPa)	G_{23} (GPa)
42.26	6.77	0.25	0.38	2.58	2.46

The transverse deformations in the 0° plies led to the highest values of the stresses (σ_{22} and σ_{33}) at the first representative element(s) of the 0° UD plies. Therefore, they were prone to affecting the laminate failure. As a summary, the FF mode was the most active of the out-resin groups 1, and the IFF mode for the out-resin group 3 (see also Fig. 6)). Out-resin group 2 would be referred to the FF mode, but no critical values were identified in it. It must be mentioned that the maximum strains for the current stress field were $\varepsilon_{11,max}^{gap} = 1.407e\text{-}03$ m/m, $\varepsilon_{11,max}^{0°\ ply} = 0.55e\text{-}03$ m/m and $\varepsilon_{22,max}^{90°\ ply} = 1.28e\text{-}03$ m/m, being lower compared to the ultimate strains of the fibre and matrix, $\varepsilon_f \approx 2.4e\text{-}02$ m/m and $\varepsilon_m = 4e\text{-}02$ m/m (Table 1).

Finally, the correlation analysis was developed, in terms of LCF, for the three out-resin groups with the elements (virtually) conditioned for one year. Fig. 14 shows that only S_{23} had a significant (linear) tendency to change results after one year of (virtual) ageing, i.e. the failure results (in out-resin group 3) generated a correlation of their values with the 20-161 conditioned inputs of the S_{23} parameter. The linearity of the tendency between the values of the failure and strength properties correlated with a factor of $R^2 = 0.86$. The strength parameter S_{12} also presented observable sensitivity forout-resin group 3. The effect was low and probably manifests local shear, anticipated largest at free edges at the weak zones. Therefore, in real structures, such as pressure vessels, it is not essential. It must be mentioned that these tendencies by the shear properties could be affected, not only by the ageing of fibre and matrix as pure constituents but also by the response of the voids under the conditioning. It has been demonstrated in the current literature that voids intensify their effects on degradation under moisture and heat conditions. However, no common results have been found due to the high dependency of the strength properties on the characteristics of laminates [30,38].

It is important to note that the conditioning of the tensile specimens was carried out on panels with the edges protected. Therefore, the ageing was not especially exaggerated on the free-edges of plies. This emphasises the significance of S_{23} in the aged filament-wound cross-ply laminated structures at low load (strain) levels. In summary, it is important to determine the degradation of S_{23} values in the composites due to chemical attack. This is also supported by the observations reported previously [2] and that stated that fibre–matrix interfaces play a role in the degradation of stiffness in GFRP cross-ply laminates [39,40]. The shear strength (e.g. S_{23}) of unidirectional composite plies is typically governed by resin behaviour and interfacial behaviour [1].

There are simply not many polymeric barrier materials that could hinder (compared to resins A and D) the diffusion, e.g., from the sides of the pure resin bending specimens (thickness 6 mm). The resins of this study are specifically designed to resist this type of chemical mediums. Typically, the idea in the sealing of edges of test specimen for conditioning is to control the direction of diffusion by a medium. In our study with the target of understanding composite material, the ageing of matrix in certain direction is not well-defined because, in the composite, the fibre–matrix interfaces and voids much affect the diffusion by the medium and this does not happen in only single clear defined direction on the ply level. A reinforcement lay-up has its own effects. In general, the degradation in the pure resin specimens was much less than in the composites and resins' strength even increased. This fact indicated that the diffusion and reactions in pure resins might be slower than in GFRP environment. For a thin barrier (e.g., Section 2 or 3 panels), the reinforcements and voids were presumed to incur potential accelerated diffusion and ageing also in the pure matrix phase between fibres. Hence, noting that the effective volume fraction of matrix was 47%, the Section 1 panel with around 10 mm barrier layer during conditioning was selected as the reference composite for the FE model of the structural layer and matrix properties estimated based on the pure matrix tests. The ageing time, to match the aged properties of the resin constituent in the composite's numerical simulation, was set equal (1 year), since no generalized method to select otherwise exist.

For the virtual conditioning, the purpose of the criterion was to predict neither damage onset of the whole model nor evolution in it by derivations of stresses, but to determine the sensitivity of the failure (ratios) values by varying the strength properties from the denominator at a fixed stress state. This is due to the target of analysing the local weak zones at the linear-elastic regime. Naturally, if the applied load level for the sensitivity analysis was higher, the sensitivity of the studied failure modes to the tensile strength (in terms of effects by X_t and Y_t) would be essential ones since the ultimate failure of the specimen simply requires sheer breakage of 0°plies. An accurate analysis of higher loads necessitates understanding the non-linear regime prior to ultimate failure, going through the damage onset. This is also important from the point of view of predicting the failure and its propagation, and therefore designing safe and properly damage-tolerant industrial structures.

In future studies, emphasis will be placed on the 3D failure criterion's implementation for a material model capable of a higher amount of stress–strain points, towards the ultimate fracture. This means the implementation of progressive damage models [41] with correlation between the elastic constants and state variables for failure modes and types applicable to the non-linear (elasto-plastic) domains.

4. Conclusions

This work studied the performance of filament-wound GFRP made of two different vinyl ester resins (Derakane 455-400 and Atlac E-Nova FW 1045). Long-term immersion conditioning in a sulphuric acid–water solution was carried out and tensile tests of non-aged and conditioned specimens were performed. A numerical multi-routine

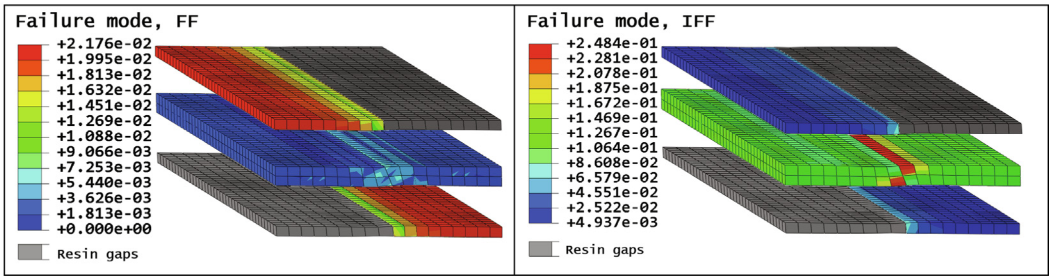

Fig. 13. Numerical results of the failure mechanism in the weak zone implemented by the Hashin 3D failure criterion with respect to the stress field (at ε_{11} = 0.67e-03 m/m) for the non-aged condition.

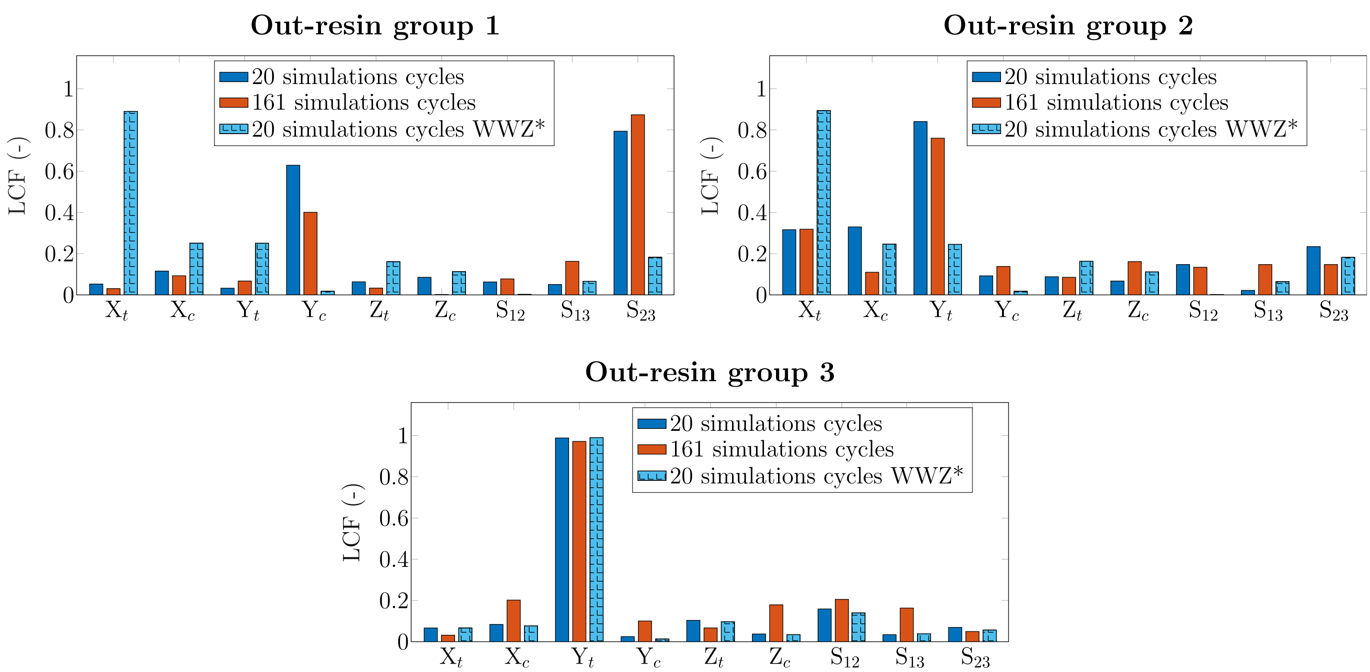

Fig. 14. Linear correlation analysis between the LCF as failure values (in their corresponding modes) and the strength properties of a ply, for each selected group of elements. * WWZ = results without Weak Zones in FE model.

approach was developed to understand the sources of degradation and failure onset upon loading, as well as the most critical strength parameters for aged GFRP. The Hashin 3D failure criterion was implemented as damage activation functions. The simulations allowed to determinate the sensitivity of the ply strength parameters at the specific amount of (virtual) ageing condition by means of a failure analysis. Based on the results, the experimental–numerical analysis led to the following conclusions:

- The flexural strength in the pure specimen of the novolac-based vinyl ester resin increased by 8%, and in the bisphenol A-based vinyl ester ones, by 33%. The values of Young's modulus decreased by 15–18%.
- GFRP specimens showed a gradual decrease in the ultimate strength throughout the whole conditioning time span of two years. The bisphenol A-based GFRP specimens presented good resistance to chemical attack in terms of ultimate strength. A marked degradation of stiffness (Young's modulus) occurred mainly during the 1-year ageing condition.
- A continuous mass increase was observed for the GFRP panels throughout the two years of conditioning. At the end of the conditioning, the mass of the panels with bisphenol A had increased by 2.36%, whereas novolac-based panels mass had increased by 1.21% on average.
- The specimens subject to the tensile tests typically showed a diagonal fracture path with an influence by the ply overlaps. These manufacturing issues of the 0°plies worked as stress concentration points and allowed us to model the weak zones in the FE model.
- The effects of ageing on the strength of the specimens were analysed by means of a 3D strength-based failure criterion in the linear-elastic region. The shear strength parameter (S_{23}) presented the highest tendency of changing results when the (GFRP-D Section 1) specimen was virtually conditioned at 1-year ageing.

5. Data availability statement

The raw/processed data required to reproduce these findings cannot be shared at this time due to technical or time limitations. The simulation re-performance outputs a significant amount of data; initialisation files are available upon request from the authors.

CRediT authorship contribution statement

G.O. Rodera: Writing - original draft, Writing - review & editing, Methodology, Software, Visualization, Data curation, Formal analysis, Investigation. **T. Pärnänen:** Validation, Resources, Writing - original draft, Writing - review & editing. **J. Jokinen:** Data curation, Software, Writing - review & editing. **M. Lindgren:** Resources, Writing - review

& editing. **E. Sarlin:** Supervision, Funding acquisition, Writing - review & editing. **M. Kanerva:** Conceptualization, Project administration, Writing - review & editing.

Declaration of Competing Interest

The authors declare that they have no known competing financial interests or personal relationships that could have appeared to influence the work reported in this paper.

Acknowledgements

This project was partly funded by the Academy of Finland postdoctoral project from micro-scale data to macro-scale understanding for improved safety of composite materials – MicMac (Grant No. 314983).

Appendix A

The equations of the Halpin-Tsai method for the ply (3D) properties of the FE model can be found in Table A.8. The two reinforcement parameters (ξ_t and ξ_s) that determine the prediction of ($E_2 = E_3$) and ($G_{12} = G_{13}$) were set to zero. Through this assumption, the constants were underestimated in the lower bound of the functions (minimum values) due to the matrix defects and manufacturing issues in the micro-structure [35].

The equations of the Hashin 3D failure criterion, implemented in the FE model for the strength loop, are given in Table A.9.

In this study, the input data matrix of the strength values for the sensitivity analysis were created by using the Optimal Latin Hypercube Sampling (OLHS). The exact values can be found in Table A.10.

Table A.8
Relationships and main parameters of the semi-empirical Halpin-Tsai method for the material definition of each ply (transversally isotropic) in the stiffness loop [2,42,27].

Engineering constants	Relationships	Other parameters
E_1	$(1-V_f)E_m + V_f E_f$	Lower bound of moduli (assumptions): $\xi_t = 0$ $\xi_s = 0$
$E_2 = E_3$	$E_m \dfrac{(1+\xi_t \eta V_f)}{(1-\eta V_f)}$	Variable for longitudinal moduli: $\eta = \dfrac{\left(\frac{E_f}{E_m}-1\right)}{\left(\frac{E_f}{E_m}+\xi\right)}$
$\nu_{12} = \nu_{13}$	$(1-V_f)\nu_m + V_f \nu_f$	The bulk moduli:
ν_{23}	$1-\nu_{21}-\frac{E_2}{(3K)}$	$K = \left[\frac{V_f}{K_f}+\frac{(1-V_f)}{K_m}\right]^{-1} \begin{cases} K_f = \frac{E_f}{3(1-2\nu_f)} \\ K_m = \frac{E_m}{3(1-2\nu_m)} \end{cases}$
$G_{12} = G_{13}$	$\dfrac{G_m(1+\xi_s \eta V_f)}{(1-\eta V_f)}$	Variable for shear moduli: $\eta = \dfrac{\left(\frac{G_f}{G_m}-1\right)}{\left(\frac{G_f}{G_m}+\xi\right)}$
G_{23}	$\dfrac{E_2}{2(1+\nu_{23})}$	

Table A.9
Invariants and failure modes of the Hashin's 3D failure criterion [20,41,21].

Invariants	$I_1 = \sigma_{11}, I_2 = \sigma_{22}+\sigma_{33}, I_3 = \tau_{23}^2 - \sigma_{22}\sigma_{33}, I_4 = \tau_{12}^2+\tau_{13}^2$
Quadratic approximation	$A_1 I_1 + B_1 I_1^2 + A_2 I_2 + B_2 I_2^2 + C_{12} I_1 I_2 + A_3 I_3 + A_4 I_4 = 1$ *
Failure modes	
FF:($\sigma_{11} > 0$)	$(\frac{\sigma_{11}}{X_t})^2 + (\frac{\tau_{12}}{S_{12}})^2 + (\frac{\tau_{13}}{S_{12}})^2 = 1$
($\sigma_{11} < 0$)	$(\frac{\sigma_{11}}{X_c})^2 = 1$
IFF: ($\sigma_{22}+\sigma_{33} > 0$)	$\dfrac{(\sigma_{22}+\sigma_{33})^2}{(Y_t)^2} - \dfrac{\sigma_{22}\cdot\sigma_{33}}{(S_{23})^2} + \dfrac{\tau_{12}^2}{S_{12}^2} + \dfrac{\tau_{13}^2}{S_{12}^2} + \dfrac{\tau_{23}^2}{S_{23}^2} = 1$
($\sigma_{22}+\sigma_{33} < 0$)	

* A_1, B_1, C_{12}, A_3 and A_4 developed in [20].

Table A.10
The conditioned (virtually) strength properties of the GFRP-D ply by means of the OLHS.

Variation	N. Case	X_t [MPa]	X_c [MPa]	Y_t [MPa]	Y_c [MPa]	Z_t [MPa]	Z_c [MPa]	S_{12} [MPa]	S_{13} [MPa]	S_{23} [MPa]
0%	0	1100	675.0	35.00	120.0	35.00	120.0	80.00	80.00	46.15
± 26%	a	937.1	893.8	43.76	128.0	27.24	131.7	79.55	84.58	52.07
	b	1028	630.6	34.54	105.8	30.86	96.31	97.89	93.69	44.33
	c	1144	524.0	38.22	90.00	32.69	115.3	66.31	70.53	50.40
	d	1375	754.9	26.25	137.4	40.07	150.0	78.94	87.37	46.76
	e	1057	737.2	27.17	118.4	29.01	112.1	62.10	64.21	49.19
	f	825.0	666.1	37.30	96.31	40.99	137.4	100.0	74.74	52.83
	g	911.8	559.5	29.01	150.0	29.94	118.4	72.63	97.89	57.69
	h	853.9	701.6	30.86	134.2	36.38	127.9	93.69	72.63	43.12
	i	969.8	612.8	33.62	146.8	38.22	99.47	83.16	85.26	35.83
	j	940.8	808.3	43.75	121.6	34.54	124.7	68.42	76.84	40.69
	k	1201	595.1	31.78	115.3	33.62	90.00	91.58	60.00	39.48
	l	1317	577.3	40.99	140.5	28.09	140.5	95.79	83.16	37.04
	m	1288	683.9	36.38	112.1	43.75	105.8	87.37	95.79	51.62
	n	1230	790.5	41.91	143.7	42.83	93.16	74.74	66.31	54.05
	o	882.9	772.7	28.09	99.47	41.91	102.6	64.21	78.94	55.27
	p	1086	719.4	29.94	93.16	39.14	143.7	76.84	81.06	38.26
	q	1346	843.8	32.69	102.6	26.25	108.9	85.26	89.47	45.55
	r	1115	648.3	35.46	131.1	35.46	134.2	70.53	68.42	34.62
	s	1259	541.8	39.14	127.9	31.78	146.8	89.47	62.10	56.48
	t	1172	506.3	40.07	108.9	37.30	121.6	60.00	100.0	41.90

Appendix B. Supplementary data

Supplementary data associated with this article can be found, in the online version, at https://doi.org/10.1016/j.compstruct.2020.113508.

References

[1] Oliveira BF, Creus GJ. An analytical–numerical framework for the study of ageing in fibre reinforced polymer composites. Compos Struct 2004;65(3–4):443–57.
[2] Kanerva M, Jokinen J, Sarlin E, Pärnänen T, Lindgren M, Järventausta M, Vuorinen J. Lower stiffness of GFRP after sulfuric acid-solution aging is due to degradation of fibre-matrix interfaces?. Compos Struct 2019;212:524–34.
[3] Davies P, Rajapakse YDS. Durability of composites in a marine environment. Netherlands: Springer; 2014.
[4] Karger-Kocsis J, Gryshchuk O. Morphology and fracture properties of modified bisphenol a and novolac type vinyl ester resins. Journal of Applied Polymer Science 2006;100(5):4012–22.
[5] Lindgren M, Wallin M, Kakkonen M, Saarela O, Vuorinen J. The influence of high-temperature sulfuric acid solution ageing on the properties of laminated vinyl-ester joints. International Journal of Adhesion and Adhesives 68 2016;68:298–304.
[6] Lindgren M, Bergman G, Kakkonen M, Lehtonen M, Jokinen J, Wallin M, et al. Failure analysis of a leaching reactor made of glass-fiber reinforced plastic. Journal of Engineering Failure Analysis 2016;60:117–36.
[7] Banna M, Shirokoff J, Molgaard J. Effects of two aqueous acidic solutions on polyester and bisphenol a epoxy vinyl ester resins. Mater Sci Eng A 2011;528 (4–5):2137–42.
[8] Kootsookos A, Burchill PJ. The effect of the degree of cure on the corrosion resistance of vinyl ester/glass fibre composites. Journal of Composites Part A: Applied Science and Manufacturing 2004;35(4):501–8.
[9] Cabral-Fonseca S, Correia JR, Rodrigues MP, Branco FA. Artificial accelerated ageing of GFRP pultruded profiles made of polyester and vinylester resins: caracterisation of physical-chemical and mechanical damage. Strain 2011;48 (2):162–73.
[10] Hull D, Clyne TW. An introduction to composite materials. 2nd ed. Cambridge University Press; 1996.
[11] Barbero EJ, Damiani TM. Phenomenological prediction of tensile strength of E-glass composites from available aging and stress corrosion data. Journal of Reinforced Plastic Composites 2003;22(4):373–94.
[12] Krishnan A, Oskay C. Modeling compression-after-impact response of polymer matrix composites subjected to seawater aging. Journal of Composite Materials 2012;46(22):2851–61.
[13] Naya F, González C, Lopes CS, Van der Veen S, Pons F. Computational micromechanics of the transverse and shear behavior of unidirectional fiber reinforced polymers including environmental effects. Compos Part A-Appl S 2016;92:146–57.
[14] Naya F, Herráez M, Lopes CS, González C, Van der Veen S, Pons F. Computational micromechanics of fiber kinking in unidirectional FRP under different environmental conditions. Compos Sci Technol 2017;144:26–35.
[15] Puck A, Schürmann H. Failure analysis of frp laminates by means of physically based phenomenological models. Compos Sci Technol 1998;58(7):1045–67.
[16] Pinho S, Dávila C.G., Camanho P.P., Iannucci L, Robinson P. Failure models and criteria for frp under in-plane or three-dimensional stress states including shear non-linearity, NASA/TM-2005-213530.
[17] Hinton MJ, Kaddour AS, Soden PD. In: Failure criteria in fibre reinforced polymer composites: the World-Wide Failure Exercise. Oxford: Elsevier Science & Techonlogy; 2004.
[18] Kaddour AS, Hinton MJ. Challenging lessons from the second world-wide failure exercise (WWFE-II): Predicting failure in polymer composite laminates under 3-D states of stress. In: 19th International Conference on Composite Materials (ICCM-19). Montreal; 2013.
[19] Hashin Z, Rotem A. A fatigue failure criterion for fiber reinforced materials. Journal of Composite Materials 1973;7(4):448–64.
[20] Hashin Z. Failure criteria for unidirectional fiber composites. J Appl Mech 1980;47 (2):329–34.
[21] Gu J, Chen P. Some modifications of Hashin's failure criteria for unidirectional composite materials. Compos Struct 2017;182:143–52.
[22] Sarlin E, Sironen R, Pärnänen T, Lindgren M, Kanerva M, Vuorinen J. The effect of matrix type on ageing of thick vinyl ester glass-fibre-reinforced laminates. Compos Struct 2017;168:840–50.
[23] Altair Engineering, Inc., ESAComp; 2018. Material database.
[24] ISO 178:2010 (e), Tech rep., Determination of flexural properties testing of plastics and polymers, International Organization for Standardization (ISO), 2011.
[25] Laurikainen P, Pötz S, Jokinen J, Essen von M, Lindgren M, Kallio P, Kanerva M, Oreski G, Sarlin E. High throughput mechanical micro-scale characterization of composites and the utilization of the results in finite element analysis, in: Proceedings of the 18th European conference on composite materials (ECCM); 2018.
[26] ISO 527-4., Tech. rep., Determination of tensile properties. Part 4: Test conditions for isotropic and orthotropic fibre-reinforced plastic composites, International Organization for Standardization (ISO) Plastics, 1997.
[27] Jones RM. Mechanics of composite materials. Taylor & Francis Inc; 1998.
[28] P. Olivier, J. Cottu, B. Ferret, Effects of cure cycle pressure and voids on some mechanical properties of carbon/epoxy laminates. Composites 1995;(26):509–15.
[29] Hancox NL. The effects of flaws and voids on the shear properties of CFRP. J Mater Sci 1977(12):884–92.
[30] Leali CM, Cerqueira MR, De Almeida SFM. Strength of hygrothermally conditioned polymer composites with voids. J Compos Mater 2005(19):97–112.
[31] W. D. Bascom, J. B. Romans, Microvoids in glass-resin composites. Their origin and effect on composite strength. Ind Eng Chem Prod Res Dev 1968;(7):172–8..
[32] Jin R, Chen W, Sudjianto A. An efficient algorithm for constructing optimal design of computer experiments. Journal of Statistical Planning and Inference 2005;134:268–87.
[33] ABAQUS/Standard User's Manual, Version 6.9, Dassault Systèmes Simulia Corp. United States; 2009.

[34] Sun CT, Quinn BJ, Tao J, Oplinger DW, William J. Comparative evaluation of failure analysis methods for composite laminates. In: Tech. rep., DOT/FAA/AR-95/109,. U.S. Department of Transportation, Office of Aviation Research; 1996.
[35] Buragohain MK. Micromechanics of a lamina. In: Composite structures. CRC Press; 2017. p. 79–132.
[36] Mittelstedt C, Becker W. Free-edge effects in composite laminates. Appl Mech Rev 2007;60(5):217–45.
[37] Davila CG, Camanho PP, Rose CA. Failure criteria for FRP laminates. Journal of Composite Materials 2005;39(4):323–45.
[38] De Almeida SFM, Dos Santos ZNN. Effect of void content on the strength of composite laminates. Compos Struct 1994(28):139–48.
[39] Sullivan JL. Creep and physical aging of composites. Compos Sci Technol 1990;39(3):207–32.
[40] Rocha IBCM, Raijmaekers S, Van der Meer FP, Nijssen RPL, Fischer HR, Sluys LJ. Combined experimental/numerical investigation of directional moisture diffusion in glass/epoxy composites. Compos Sci Technol 2017;151:16–24.
[41] Camanho PP, Matthews FL. A progressive damage model for mechanically fastened joints in composite laminates. Journal of Composite Materials 1999;33(24):2248–80.
[42] Fragoudakis R. Failure analysis and prevention: Failure concepts in fiber reinforced plastics. InTech; 2017.